SCIENTIFIC REPORTS

OPEN

The influence of electrical effects on device performance of organic solar cells with nano-structured electrodes

Received: 31 October 2016
Accepted: 1 June 2017
Published online: 13 July 2017

Mina Mirsafaei[1], Amir Hossein Fallahpour[2], Paolo Lugli[2], Horst-Günter Rubahn[1], Jost Adam[1] & Morten Madsen[1]

Integration of light-trapping features and exploitation of metal nanostructure plasmonic effects are promising approaches for enhancing the power conversion efficiency of organic solar cells. These approaches' effects on the light absorption enhancement have been widely studied, especially in inorganic devices. While this light-trapping concept can be transferred to organic devices, one has to also consider nanostructure-induced electrical effects on the device performance, due to the fundamental difference in the organic semiconducting material properties compared to their inorganic counterparts. In this contribution, we exemplarily model the electrical properties of organic solar cells with rectangular-grating structures, as compared to planar reference devices. Based on our numeric results, we demonstrate that, beyond an optical absorption enhancement, the device fill factor improves significantly by introducing the grating structures. From the simulations we conclude that enhanced carrier collection efficiency is the main reason for the increased solar cell fill factor. This work contributes towards a more fundamental understanding of the effect of nanostructured electrodes on the electrical properties of organic solar cells.

Low material and fabrication cost, the ease of processing organic materials and the possibility of making ultra-thin, flexible cells using techniques, such as solution processes[1,2], printing[3,4] and roll-to-roll technology[5], render organic solar cells (OSCs) ideal candidates for the future renewable energy market. The organic material properties, such as the molecular mass[6], the band gap and absorption properties[7,8], can easily be tailored through modifying the length and presence of different functional groups[9], which makes them interesting for a wide range of opto-electronic applications. In recent years, performance improvements of organic solar cells have led to high power conversion efficiencies (PCE)[10–13], currently having a record of 13.2%, set by Heliatek. Nevertheless, organic photoactive materials come with certain inherent drawbacks such as a relatively narrow absorption band, short exciton diffusion lengths and low charge carrier mobility[14].

To meet these drawbacks and to further increase the device efficiency, various light management techniques have been investigated to achieve optical field enhancement in the photoactive layer region. These approaches are based on plasmonic, diffraction and scattering effects, e.g., introduced by the integration of metallic nanoparticles near or in the photoactive layer, by the inclusion of metallic and non-metallic, aperiodic or (quasi-) periodic surface structures, or by the integration of randomly distributed metallic nanoparticles in the back contact layer[15–17]. There are several reports on nanostructured inorganic solar cell efficiency improvements as a result of enhanced optical absorption, which is a dominant factor to increase the overall performance and, in this case, directly translates to an increased photocurrent[18]. Less attention has been paid to the electrical effect from incorporation of plasmonic nanostructures in inorganic solar cells, due to the large photoactive layer thickness, very high charge carrier mobility, and efficient charge collection efficiency. It has however recently been demonstrated that nanostructures can lead to improved electrical properties in inorganic solar cells, focusing mainly on the improved electrical contacting arising from the different nanostructures[19]. In organic devices, due to the

[1]SDU NanoSYD, Mads Clausen Institute, University of Southern Denmark, Alsion 2, Sønderborg, DK-6400, Denmark. [2]Department of Electrical and Computer Engineering, Institute for Nanoelectronics, Technical University of Munich, Arcisstr, 21 80333, Munich, Germany. Correspondence and requests for materials should be addressed to M.M. (email: madsen@mci.sdu.dk)

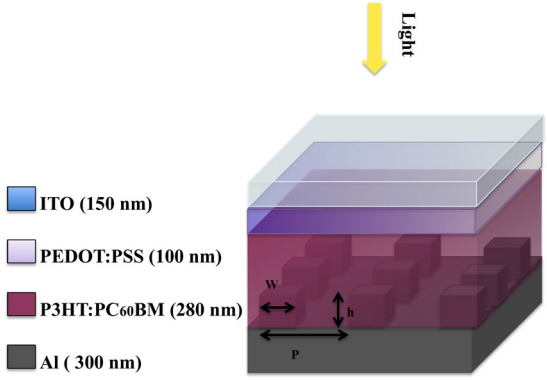

Figure 1. Organic solar cell model geometry, with a back contact grating and material thicknesses as used in the simulations (h – pillar height [nm], p – grating period [nm], w – pillar width [nm]).

fundamental differences between the opto-electronic properties of the organic semiconductors and inorganic materials, it becomes necessary to also consider improvements coming from the electrical properties introduced by nanostructures, alongside the optical absorption enhancement[20–22].

Although the electrical processes taking place in organic solar cells, e.g., the exciton generation/dissociation, charge carrier transport, recombination loss mechanisms, and interfacial morphology effects, have been experimentally investigated for nanostructured OSCs[23–27], a theoretical/numerical study for a comprehensive prediction of electrical effects arising from the integration of such complex non-planar nanostructures is, to date, still missing.

The integrated light-trapping nanostructures are likely to affect physical processes such as charge carrier losses, transport and collection efficiency. These processes depend on several factors, such as the electric field distribution, the exciton separation process and the spatial concentration dependence of carrier recombination, effectively influencing the final PCE of the cell.

To address the issue of tracing the electrical device properties more accurately, we perform numerical simulations of nanostructured organic solar cells, considering the involved underlying organic semiconductor physics. We compute the optical and electrical device properties, using three-dimensional (3D) finite-difference time-domain (FDTD) and finite element (FE) methods, respectively. In particular, we investigate the contact behavior, the exciton dynamics, and the charge carrier transport for disordered materials. Building on that, as a case study, we perform full electrical simulations of a well-known conventional organic solar cell setup with a back contact grating structure, to understand how nanostructuring influences the electrical properties of such organic devices. As a result, we find a significant improvement of the electrical properties in the investigated nanostructured organic solar cell, beyond what is governed by the optical absorption enhancements, originating merely from the implemented grating structure.

Results and Discussion

The exemplary chosen conventional OSC structure studied in this work is composed of the following well-known multilayer structure (Fig. 1): Indium thin oxide (ITO)/poly-3,4-ethylenedioxythiophene:poly(styrenesulfonate) (PEDOT:PSS) /Poly(3-hexylthiophene-2,5-diyl)(P3HT) blended with [6,6]-phenyl C61 butyric acid methyl ester($PC_{60}BM$)/Aluminum(Al).

In our study, in order to first investigate simulation parameter consistency and to verify our electrical model, we fitted the model to experimentally measured data for a planar reference device structure[28]. All electrical parameters used for the fitting are directly taken from the literature or estimated by experimental measurements (Table 1). Figure 2 demonstrates the established agreement between the experimental and simulated results for current density versus voltage (*J-V*) curves for a planar organic solar cell with a 200 nm thick active layer.

As a second step, in order to accurately trace the organic solar cell electrical properties, we applied a uniform, constant exciton generation profile in the active layer, allowing for a precise electrical device response analysis. We performed electrical simulations for the modified devices with varying grating geometries, and we compared the results to those of the planar reference structure. We considered a back contact grating architecture (see Fig. 1) with different square pillar heights ($h = 40$, 80, 120, 160 and 200 nm), while keeping the grating pitch ($p = 400$ nm) and the pillar width ($w = 100$ nm) constant. Figure 3 shows the simulated device current density versus voltage (*J-V*) characteristics for different pillar heights. The pillar influence on the open circuit voltage V_{oc} is very limited, while the short circuit current density J_{sc} is decreasing for taller pillars. This reduction is in line with our expectations, since the active layer height in this simulation is kept constant, and an increased pillar height consequently leads to a reduced effective active layer volume. The reduced active layer volume leads to a lower absorption of light, which, in effect, also decreases J_{sc} for increasing pillar heights. This is also the main driver for the decreasing PCE obtained for increasing pillar heights in these simulations. To understand the electrical response of the grating architecture, Fig. 4 depicts the calculated, commonly used, figures of merit, i.e., V_{oc}, J_{sc}, fill factor (FF) and PCE, as functions of the pillar height.

The observed PCE reduction, however, is not consistent with the contribution coming from the lower absorption, and hence J_{sc}. This observation can be understood by considering the improved collection efficiency, leading

Description	Parameter	Value	Ref.
Photoactive layer thickness	L	200 nm	
Cathode (Al) work function	$\Phi_{cathode}$	− 4.1	42
Anode (PEDOT) work function	Φ_{anode}	−5.2	43
HOMO level onset	E_{HOMO}	−5.1 eV	44–46
LUMO level onset	E_{LUMO}	−3.9 eV	44–46
Decay rate of excitons	k_{dec}	10^4 1/s	Fit with *J-V* experiment
Pair separation distance	x_a	1.2 nm	Fit with *J-V* experiment
Width of LUMO and HOMO Gaussian	σ_e, σ_h	0.128 eV	47–49
Hole mobility	μ_h	4×10^{-4} cm^2/V.s	50–52
Electron mobility	μ_e	2×10^{-3} cm^2/V.s	50–52

Table 1. Electrical simulation parameters.

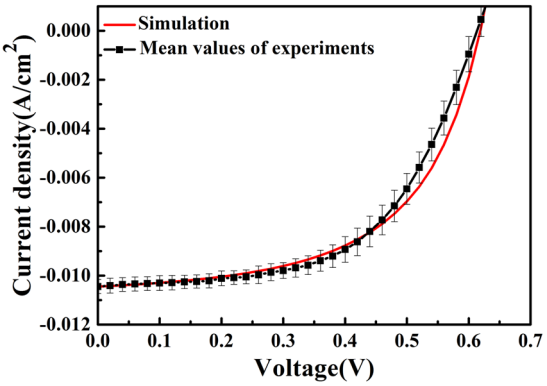

Figure 2. Experimental[28] and simulated results for current density versus voltage curves for a planar organic solar cell with a 200 nm thick active layer. Our model widely agrees with the experimental results.

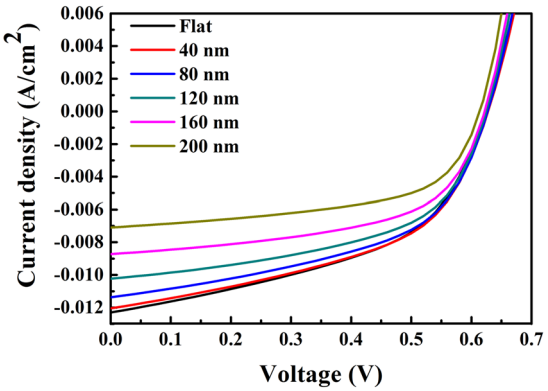

Figure 3. Current density versus voltage (*J-V*) characteristic of the flat OSC, compared to the devices with back contact grating of varying height. For an increased pillar height, J_{sc} (in magnitude), V_{oc} and PCE decrease. On the other hand, the FF increases with increasing nano-structure height. (Higher *Jsc* compared to Fig. 2 is due to larger active layer thickness (280 nm).

to a fill factor (FF) improvement with increased pillar height in the cells. As shown in Fig. 4, a significant FF improvement of 18% can be observed when increasing the grating structure height to 200 nm. This FF improvement is mainly related to an increased interfacial area for collecting charge carriers between the active layer and the back contact, as well as the reduced losses during the free charge carrier transport towards the contact. This FF increase leads to a smaller PCE drop as compared to the one arising solely from the drop in J_{sc}. Accordingly, as shown in Fig. 5 for the simulated electron collection path and spatial magnitude of the electron current,

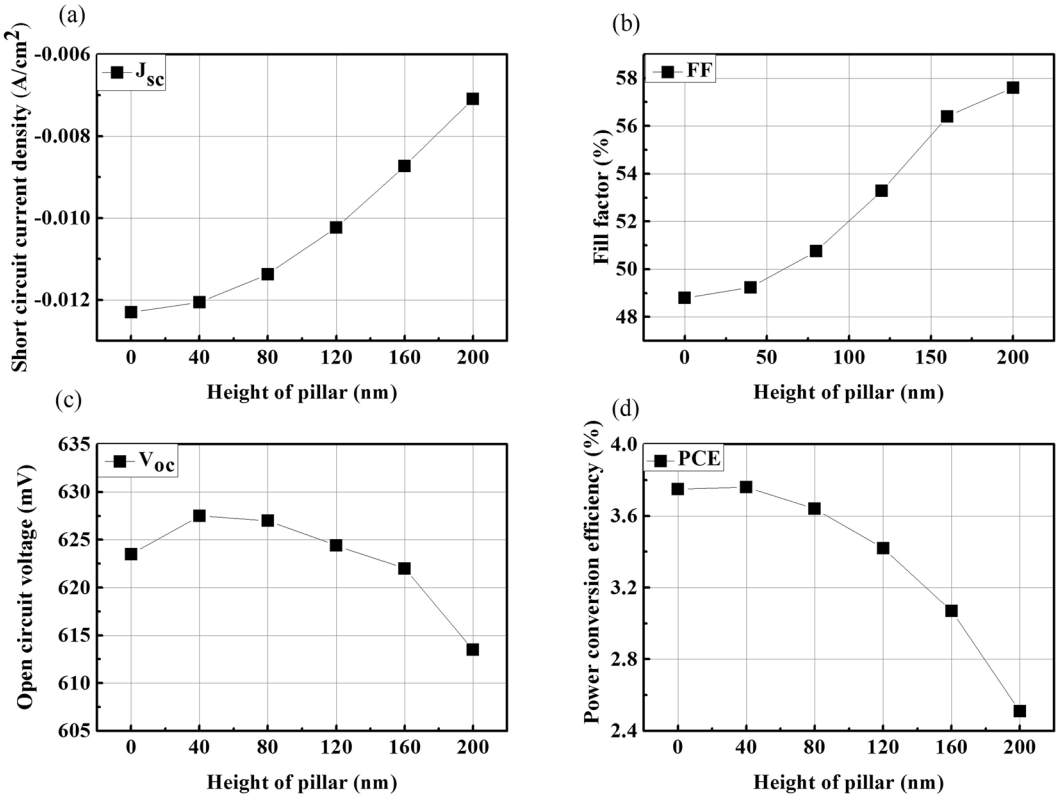

Figure 4. Numerical results for (**a**) the short circuit current density J_{sc}, (**b**) the fill factor FF, (**c**) the open circuit voltage V_{oc}, and (**d**) the overall power conversion efficiency PCE of the considered OSC as functions of varying pillar height. While the effect on *V*oc is limited, J_{sc} decreases noticeably for higher pillars. This decrease is addressed to the fact that in our simulations the active layer thickness (and not volume) is kept constant, which reduces the active layer volume of the absorbing material with increasing pillar height. However, the PCE reduction is not consistent with the lower absorption, which can be understood by considering the improved collection efficiency and thus, FF enhancement as a function of pillar height.

introducing pillars leads to a more efficient collection of free carriers and hence to a better FF in comparison to the planar cell.

The simulations show that even with an increased FF, the overall PCE in the structured cell is reduced as compared to the planar one (Fig. 4d). This is due to the fact that we use a constant generation profile to examine the electrical behavior of these structures, and thus by introducing the grating structure, the amount of photo-generated carriers is reduced along with the volume of the absorber, which consequently results in lower PCE.

In reality, however, several experimental and numerical studies show that even if the integration of nanoparticles or grating structures into the cells reduces the absorber volume, this introduction can still enhance the overall optical absorption efficiency and thus the cell's J_{sc}[29–31]. In order to shed light on this discrepancy, finally, we perform optical simulations for same geometries, and subsequently introduce spatially resolved exciton generation rates to our electrical simulator. As shown in Fig. 6a, the optical absorption spectrum calculated for an organic active layer that includes square pillars of height 200 nm shows 8.8% optical absorption enhancement (averaged over the considered wavelength range) compared to a planar solar cell. We note that this is the highest optical absorption enhancement obtained when comparing numerous different pillar heights and widths for 2 different investigated grating pitches. We show the optical absorption enhancement for the different pillar dimensions in Figure S1 in the supplementary information. Figure 6b compares the *J-V* characteristics of the grating-structured cell (blue curve) to the one having a planar geometry (black curve), where the grating structure-influenced exciton generation profile is equalized with the planar one. This shows that the power conversion efficiency for an OSCs comprising a nanostructured grating is enhanced significantly due to improved charge collection efficiency only, i.e., without including the optical (8.8%) enhancement. It should be noted that the PCE could practically improve to higher values through detailed opto-electrical engineering, due to the concurrent optical and electrical improvement offered by this technology. To this end, we simulated the device again, considering the 8.8% optical enhancement (red curve). As demonstrated in Table 2 and by the *J-V* curve (Fig. 6(b)), the PCE increased by up to 28.5%, resulting from both optical absorption enhancement and improved charge collection efficiency. We provide the solar cell performance parameters for different pillar heights, including both the optical absorption and the electrical enhancement, in table S1 in the supplementary information. The maximum J_{sc} and FF occurs at a pillar height of 200 nm.

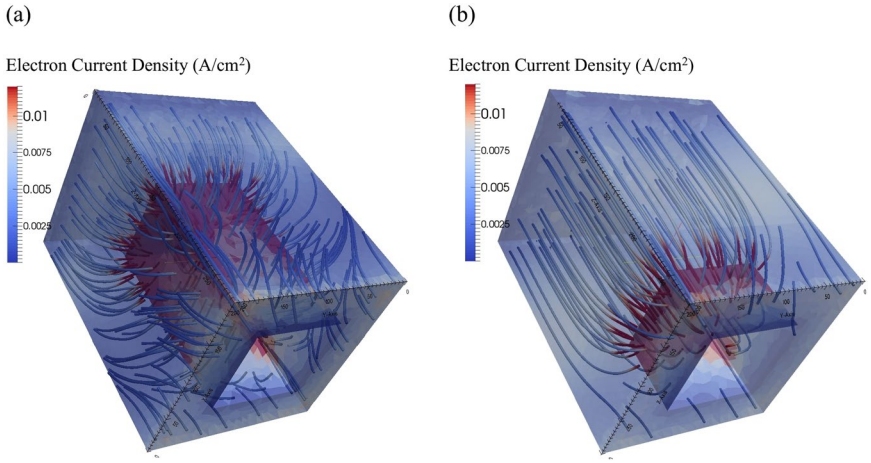

Figure 5. Electron current density magnitude (tubes) within the active layer for two different pillar heights (**a**) h = 200 nm, (**b**) h = 80 nm. By introducing pillars in the organic solar cell, the surface area between the active layer and the back contact increases. This effectively leads to a more efficient free carrier collection and hence to an increased FF as compared to the planar reference cell.

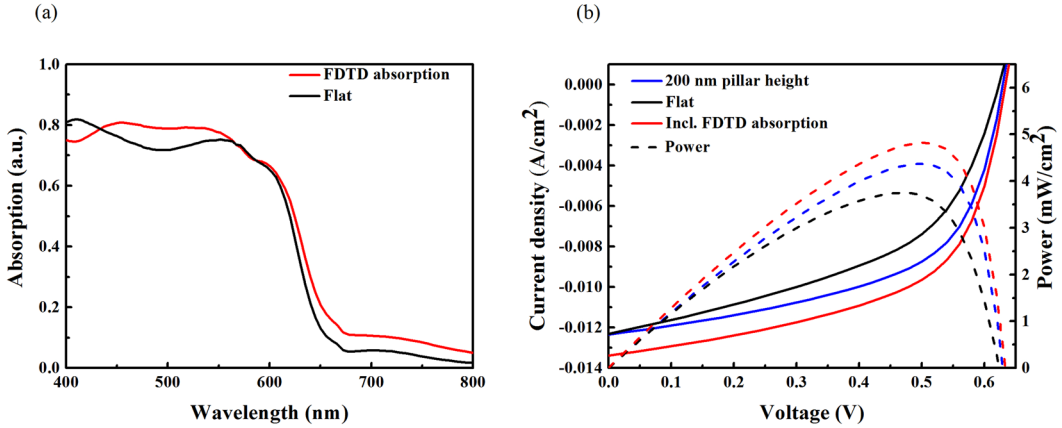

Figure 6. (**a**) Optical absorption of planar and square grating structures with a pillar height of 200 nm. The organic active layer that includes square pillars of height 200 nm shows an 8.8% optical absorption enhancement (averaged over the considered wavelength range). (**b**) Electrical properties of the planar reference solar cell (black line), the grating structure with optical generation profile equalized to the planar cell (blue line) and the solar cell with optical generation profile calculated by the FDTD method (red line). The power conversion efficiency for OSCs having a nano-structured grating enhances, exclusively due to the improved charge collection efficiency. By incorporating the 8.8% optical enhancement within the solar cell, the electrical properties in terms of J_{sc}, FF and thus PCE (28.5%) improve even further.

Device	V_{oc} (mV)	J_{sc} (mA/cm²)	FF (%)	PCE (%)
Planar	623	12.3	48.8	3.74
200 nm pillars	629	12.3	56.5	4.37
200 nm pillars Incl. optical absorption enhancement	629	13.3	57.6	4.82*

Table 2. Characteristics of the organic solar cell shown in Fig. 6b. *Overall PCE improvement (~28.5%) is due to better charge collection efficiency (~18%) and optical enhancement (~8.8%).

In general, our approach is applicable to several complex geometries and material systems. By comparing the results obtained with experimental measurements of similar structures, the calculated absorption and FF enhancement can be qualitatively validated[31–35]. For example, for similar structures to those studied here, it has been shown experimentally in ref. 30 that cell performance and FF is enhanced (25.5% and 19.4%, respectively) by nano-patterned PEDOT:PSS, using nano-imprint lithography, which can be explained qualitatively with our analogous simulation study.

Conclusion

In this work we have studied the electrical properties of three-dimensional organic solar cells with a back contact grating structure. We have demonstrated that the cells structured with square pillars can lead to a 18% fill factor enhancement as compared to the planar OSC. We address this fill factor enhancement to an increased interfacial area for collecting charge carriers, which results in reduced losses and improved charge collection efficiency. The highest fill factor for the studied structure is found when the grating height is at the tested maximum of 200 nm, which is achievable with several available lithography techniques. In addition, optical simulations show an 8.8% absorption enhancement inside the active layer. Our results confirm that, by implementing nanostructured gratings in organic solar cells, beyond optical enhancement, we are able to increase the power conversion efficiency of solar cells due to a concurrent enhancement of both the electrical and optical cell characteristics.

Methods

Electrical simulation. For exciton dynamics and free charge transport, we developed a comprehensive numerical model, based on the drift-diffusion approximation and a variant of Koster *et al.*'s[36] concept of exciton continuity. Our model includes several fundamental physical processes specifically associated to organic semiconductors that allow us to consider the effect of energetic disorder and electrode properties. The developed model (a detailed mathematical description can be found in ref. 28) overcomes most of the common approximations previously used in simulating the opto-electrical properties of OSCs. One important feature of our approach is that we apply a reliable model at the organic-metal interfaces, using a combination of the Mott-Schottky and the Scott-Malliaras model. Furthermore, we consider the fundamental difference between carrier transport in inorganic semiconductors (which assume the presence of a well-defined energy band edge) and in organic semiconductors (which include a hopping mobility model and a Gaussian density of states model). Such a modification is significant for a reliable approximation of organic semiconductors, which consist of disordered polymeric or molecular structures bonded by weak Van der Waals interactions. The main simplification in our approach is that the model treats the active layer as a single bulk hetero-junction (BHJ) material, considering an effective medium approximation, where the real interfaces between donor and acceptor are not explicitly considered. Since the simulation of realistic donor/acceptor blend morphology is computationally expensive and requires several input parameters that cannot be derived by measurements, this simplification is common in the drift-diffusion approach for BHJ layer modeling.

Optical Simulation. We performed the optical analysis using the FDTD method, employing the commercially available *FDTD Solutions* software package from Lumerical to calculate the spatial electromagnetic field distribution, versus time and position, in a 3D domain. We employed periodic (Bloch) boundary conditions for the lateral (x- and y-) directions, and perfectly matched layer (PML) boundary conditions at the contacts in the vertical (z-) direction. As illumination source, we used a normally incident plane wave polarized along the x-axis. In order to address the plasmonic behavior correctly, we chose a spatial mesh size of 4 nm in the regions surrounding the nanostructures. We chose the material refractive indices according to the literature[37–40]. We normalized the results to the air mass (AM) 1.5 spectrum. Based on the calculated electric field intensity profile at each incident wavelength inside the organic active layer, the number of photons absorbed can be calculated by

$$G(\lambda) = \frac{|E(\lambda)|^2 \, imag(\varepsilon)}{2\hbar} \tag{1}$$

where the E is electric field, ε is a electric permittivity, λ denotes the wavelength and $\hbar$ is the reduced Planck constant. Assuming that each absorbed photon generates an exciton in OSCs, we subsequently calculate the exciton generation rate inside the organic active layer, by integrating $G(\lambda)$ over the incident light spectrum[39,41].

References

1. Chen, C.-C. *et al.* Visibly transparent polymer solar cells produced by solution processing. *ACS Nano* **6**, 7185–7190 (2012).
2. Kang, J.-W. *et al.* Fully spray-coated inverted organic solar cells. *Solar Energy Materials and Solar Cells* **103**, 76–79 (2012).
3. Krebs, F. C. Fabrication and processing of polymer solar cells: A review of printing and coating techniques. *Solar Energy Materials and Solar Cells* **93**, 394–412 (2009).
4. Shaheen, S. E., Radspinner, R., Peyghambarian, N. & Jabbour, G. E. Fabrication of bulk heterojunction plastic solar cells by screen printing. *Applied Physics Letters* **79**, 2996–2998 (2001).
5. Søndergaard, R., Hösel, M., Angmo, D., Larsen-Olsen, T. T. & Krebs, F. C. Roll-to-roll fabrication of polymer solar cells. *Materials Today* **15**, 36–49 (2012).
6. Ma, W., Kim, J. Y., Lee, K. & Heeger, A. J. Effect of the molecular weight of poly (3-hexylthiophene) on the morphology and performance of polymer bulk heterojunction solar cells. *Macromolecular rapid communications* **28**, 1776–1780 (2007).
7. Hoppe, H. & Sariciftci, N. S. Organic solar cells: An overview. *Journal of Materials Research* **19**, 1924–1945 (2004).
8. Dennler, G., Scharber, M. C. & Brabec, C. J. Polymer-Fullerene Bulk-Heterojunction Solar Cells. *Advanced Materials* **21**, 1323–1338 (2009).
9. Chen, H.-Y. *et al.* Polymer solar cells with enhanced open-circuit voltage and efficiency. *Nature Photonics* **3**, 649–653 (2009).
10. He, Z. *et al.* Enhanced power-conversion efficiency in polymer solar cells using an inverted device structure. *Nature Photonics* **6**, 593–597 (2012).
11. Li, G., Zhu, R. & Yang, Y. Polymer solar cells. *Nature Photonics* **6**, 153–161 (2012).
12. Dou, L. *et al.* Tandem polymer solar cells featuring a spectrally matched low-bandgap polymer. *Nature Photonics* **6**, 180–185 (2012).
13. Li, N. *et al.* Towards 15% energy conversion efficiency: A systematic study of the solution-processed organic tandem solar cells based on commercially available materials. *Energy & Environmental Science* (2013).
14. Sungmo, A., Devin, R. & Wounjhang, P. Plasmonic nanostructures for organic photovoltaic devices. *Journal of Optics* **18**, 033001 (2016).
15. Pala, R. A. *et al.* Optimization of non-periodic plasmonic light-trapping layers for thin-film solar cells. *Nat Commun* **4** (2013).
16. Müller-Meskamp, L. *et al.* Efficiency Enhancement of Organic Solar Cells by Fabricating Periodic Surface Textures using Direct Laser Interference Patterning. *Advanced Materials* **24**, 906–910 (2012).

17. De Oliveira Hansen, R. M., Liu, Y., Madsen, M. & Rubahn, H.-G. Flexible organic solar cells including efficiency enhancing grating structures. *Nanotechnology* **24**, 145301 (2013).
18. Lin, H. *et al*. Rational Design of Inverted Nanopencil Arrays for Cost-Effective, Broadband, and Omnidirectional Light Harvesting. *ACS Nano* **8**, 3752–3760 (2014).
19. Liang, X. *et al*. Inverted Silicon Nanopencil Array Solar Cells with Enhanced Contact Structures. *Scientific Reports* **6**, 34139 (2016).
20. Ray, B., Khan, M. R., Black, C. & Alam, M. A. Nanostructured Electrodes for Organic Solar Cells: Analysis and Design Fundamentals. *IEEE Journal of Photovoltaics* **3**, 318–329 (2013).
21. Baek, S.-W. *et al*. Au@Ag Core–Shell Nanocubes for Efficient Plasmonic Light Scattering Effect in Low Bandgap Organic Solar Cells. *ACS Nano* **8**, 3302–3312 (2014).
22. Park, H. I. *et al*. High Performance Organic Photovoltaics with Plasmonic-Coupled Metal Nanoparticle Clusters. *ACS Nano* **8**, 10305–10312 (2014).
23. Zampetti, A. *et al*. Influence of the interface material layers and semiconductor energetic disorder on the open circuit voltage in polymer solar cells. *Journal of Polymer Science Part B: Polymer Physics* **53**, 690–699 (2015).
24. Wang, C. C. D. *et al*. Optical and electrical effects of gold nanoparticles in the active layer of polymer solar cells. *Journal of Materials Chemistry* **22**, 1206–1211 (2012).
25. Fung, D. D. S. *et al*. Optical and electrical properties of efficiency enhanced polymer solar cells with Au nanoparticles in a PEDOT-PSS layer. *Journal of Materials Chemistry* **21**, 16349–16356 (2011).
26. Sha, W. E. I., Choy, W. C. H. & Cho Chew, W. The roles of metallic rectangular-grating and planar anodes in the photocarrier generation and transport of organic solar cells. *Applied Physics Letters* **101**, 223302 (2012).
27. Sha, W. E. I., Li, X. & Choy, W. C. H. Breaking the Space Charge Limit in Organic Solar Cells by a Novel Plasmonic-Electrical Concept. *Scientific Reports* **4**, 6236 (2014).
28. Fallahpour, A. H. *et al*. Modeling and simulation of energetically disordered organic solar cells. *Journal of Applied Physics* **116**, 184502 (2014).
29. Lim, E. L. *et al*. A review of recent plasmonic nanoparticles incorporated P3HT: PCBM organic thin film solar cells. *Organic Electronics* **36**, 12–28 (2016).
30. Choi, J.-H. *et al*. Enhancement of organic solar cell efficiency by patterning the PEDOT:PSS hole transport layer using nanoimprint lithography. *Organic Electronics* **14**, 3180–3185 (2013).
31. Pandey, A. K., Aljada, M., Velusamy, M., Burn, P. L. & Meredith, P. Nanostructured, Active Organic–Metal Junctions for Highly Efficient Charge Generation and Extraction in Polymer-Fullerene Solar Cells. *Advanced Materials* **24**, 1055–1061 (2012).
32. Li, X. *et al*. Polarization-independent efficiency enhancement of organic solar cells by using 3-dimensional plasmonic electrode. *Applied Physics Letters* **102**, 153304 (2013).
33. Li, X. *et al*. Dual Plasmonic Nanostructures for High Performance Inverted Organic Solar Cells. *Advanced Materials* **24**, 3046–3052 (2012).
34. Lee, J. H. *et al*. Enhanced Solar-Cell Efficiency in Bulk-Heterojunction Polymer Systems Obtained by Nanoimprinting with Commercially Available AAO Membrane Filters. *Small* **5**, 2139–2143 (2009).
35. Li, X. H., Sha, W. E. I., Choy, W. C. H., Fung, D. D. S. & Xie, F. X. Efficient Inverted Polymer Solar Cells with Directly Patterned Active Layer and Silver Back Grating. *The Journal of Physical Chemistry C* **116**, 7200–7206 (2012).
36. Koster, L. J. A., Smits, E. C. P., Mihailetchi, V. D. & Blom, P. W. M. Device model for the operation of polymer/fullerene bulk heterojunction solar cells. *Physical Review B* **72**, 085205 (2005).
37. Burkhard, G. F., Hoke, E. T. & McGehee, M. D. Accounting for interference, scattering, and electrode absorption to make accurate internal quantum efficiency measurements in organic and other thin solar cells. *Advanced Materials* **22**, 3293–3297 (2010).
38. He, Z. *et al*. Enhanced power-conversion efficiency in polymer solar cells using an inverted device structure. *Nat Photon* **6**, 591–595 (2012).
39. Monestier, F. *et al*. Modeling the short-circuit current density of polymer solar cells based on P3HT:PCBM blend. *Solar Energy Materials and Solar Cells* **91**, 405–410 (2007).
40. Tumbleston, J. R., Ko, D. H., Samulski, E. T. & Lopez, R. Absorption and quasiguided mode analysis of organic solar cells with photonic crystal photoactive layers. *Opt Express* **17**, 7670–7681 (2009).
41. Karakasoglu, I., Wang, K. X. & Fan, S. Optical-Electronic Analysis of the Intrinsic Behaviors of Nanostructured Ultrathin Crystalline Silicon Solar Cells. *ACS Photonics* **2**, 883–889 (2015).
42. Brown, T. M. *et al*. Time dependence and freezing-in of the electrode oxygen plasma-induced work function enhancement in polymer semiconductor heterostructures. *Organic Electronics* **12**, 623–633 (2011).
43. Brown, T. M. *et al*. Built-in field electroabsorption spectroscopy of polymer light-emitting diodes incorporating a doped poly(3,4-ethylene dioxythiophene) hole injection layer. *Applied Physics Letters* **75**, 1679–1681 (1999).
44. Scharber, M. C. *et al*. Design Rules for Donors in Bulk-Heterojunction Solar Cells—Towards 10% Energy-Conversion Efficiency. *Advanced Materials* **18**, 789–794 (2006).
45. Kim, J. Y. *et al*. New Architecture for High-Efficiency Polymer Photovoltaic Cells Using Solution-Based Titanium Oxide as an Optical Spacer. *Advanced Materials* **18**, 572–576 (2006).
46. Baek, W.-H. *et al*. Effect of P3HT:PCBM concentration in solvent on performances of organic solar cells. *Solar Energy Materials and Solar Cells* **93**, 1263–1267 (2009).
47. Moehl, T. *et al*. Relaxation of Photogenerated Carriers in P3HT:PCBM Organic Blends. *ChemSusChem* **2**, 314–320 (2009).
48. Garcia-Belmonte, G. *et al*. Influence of the Intermediate Density-of-States Occupancy on Open-Circuit Voltage of Bulk Heterojunction Solar Cells with Different Fullerene Acceptors. *The Journal of Physical Chemistry Letters* **1**, 2566–2571 (2010).
49. Garcia-Belmonte, G., Boix, P. P., Bisquert, J., Sessolo, M. & Bolink, H. J. Simultaneous determination of carrier lifetime and electron density-of-states in P3HT:PCBM organic solar cells under illumination by impedance spectroscopy. *Solar Energy Materials and Solar Cells* **94**, 366–375 (2010).
50. Torricelli, F., Kovács-Vajna, Z. M. & Colalongo, L. The role of the density of states on the hole mobility of disordered organic semiconductors. *Organic Electronics* **10**, 1037–1040 (2009).
51. Tanase, C., Meijer, E. J., Blom, P. W. M. & de Leeuw, D. M. Unification of the Hole Transport in Polymeric Field-Effect Transistors and Light-Emitting Diodes. *Physical Review Letters* **91**, 216601 (2003).
52. Garcia-Belmonte, G. *et al*. Charge carrier mobility and lifetime of organic bulk heterojunctions analyzed by impedance spectroscopy. *Organic Electronics* **9**, 847–851 (2008).

Acknowledgements

A.H.F. and P.L. acknowledge the "LORIX-Large Organic Robust Imager for X-Ray Sensing (HORIZON 2020-N° 644103)" project for financial support. In addition, M. Mirsafaei, H.-G.R. and M. Madsen acknowledge the European Union Seventh Framework Programme n°607232 [THINFACE], the Innovation Fund Denmark under the project "SunTune" and the RollFlex project, which is financed by Interreg Deutschland-Danmark with means from the European Regional Development Fund, for their financial support. The work is performed within the PCAM European doctorate. The authors would like to appreciate the helpful guidance of Professor Aldo di Carlo in manuscript preparation.

Author Contributions

A.H.F. and M. Mirsafaei contributed equally to this work, which was supervised by P.L., H.-G.R., J.A. and M. Madsen. M. Mirsafaei provided the optical simulations and A.H.F. performed the electrical simulations. All authors contributed to writing and reviewing the manuscript.

Additional Information

Supplementary information accompanies this paper at doi:10.1038/s41598-017-05591-8

Competing Interests: The authors declare that they have no competing interests.

Publisher's note: Springer Nature remains neutral with regard to jurisdictional claims in published maps and institutional affiliations.